SnO_2-rGO nanocomposite as an efficient electron transport layer for stable perovskite solar cells on AZO substrate

Rong Liu[1], **Renzheng Qiu**[1], **Taoyu Zou**[1], **Chuan Liu**[2], **Jun Chen**[2], **Qing Dai**[3], **Shengdong Zhang**[1] **and Hang Zhou**[1,3]

[1] School of Electronic and Computer Engineering, Shenzhen Graduate School, Peking University, Shenzhen, 518055, People's Republic of China
[2] State Key Laboratory of Optoelectronic Materials and Technologies, Sun Yat-sen University, Guangzhou 510275, People's Republic of China
[3] National Center for Nanoscience & Technology, Chinese Academy of Sciences, Beijing 100190, People's Republic of China

E-mail: zhouh81@pkusz.edu.cn

Abstract

Electron transport layer (ETL) plays an important role in realizing efficient and stable perovskite solar cells (PSCs). There are continuous efforts in developing new types of low cost ETLs with improved conductivity and compatibility with perovskite and the conducting electrode. Here, in order to obtain high efficient and stable PSCs on ZnO:Al (AZO) substrate, reduced graphene oxide (rGO) is incorporated into SnO_2 nanoparticles to form composite ETL. For planar PSC on AZO substrates, SnO_2-rGO with a low incorporation ratio of 3 wt% rGO significantly enhances the device short circuit current density (J_{sc}) and the fill factor when compared to the device with pristine SnO_2 ETL, leading to an overall power conversion efficiency of 16.8% with negligible hysteresis. The effectiveness of the excited charge transfer process of SnO_2-rGO ETL is revealed by time-resolved photoluminescence decay, and by electrochemical impedance spectrum measurements. Furthermore, the solar cell stability is also enhanced due to the incorporation of rGO in the ETL. This work provides a low cost and effective ETL modification strategy for achieving high performance planar PSCs.

Supplementary material for this article is available online

Keywords: AZO substrate, electron transport layer, electrochemical impedance spectroscopy, solar cell, graphene, metal oxide

(Some figures may appear in colour only in the online journal)

1. Introduction

Perovskite solar cells (PSCs), with a power conversion efficiency (PCE) reaching 23.3% [1], have attracted great attention in recent years. The remarkable achievement of PSC is owing to the excellent material properties of perovskite, such as suitable bandgap, high carrier mobility and a long diffusion length [2–4]. The improvement of interfacial and hole/electron transporting layer also make a significant contribution to this rapid development. TiO_2 is one of the most widely adopted electron transport layers (ETLs). Nonetheless, the fact that TiO_2 requires a high temperature sintering process makes it unfavorable for practical application. Even worse, the photocatalytic active TiO_2 could lead to photodegradation of perovskite material [5]. ZnO [6–9] and SnO_2 [10–13] are also being studied as alternative low cost ETL candidates. It is reported that ZnO surface usually contains hydroxide and the residual acetate ligands that can also decompose the perovskite film, adding to the device instability [14]. Among many n-type metal oxide, SnO_2 with suitable conduction band level and excellent mobility is found to be a better electron transportation for PSCs [15]. PSCs with SnO2 ETL has achieved a certified efficiency of 20% [16]. A recent report yttrium (Y)-doped SnO_2 NSAs, results exhibit improved performance with much reduced hysteresis [17]. In addition, lithium (Li) and Stibium (Sb) doped SnO_2 films also have been successfully reported [18, 19].

Here, we report our investigation on reduced graphene oxide (rGO) incorporated SnO_2 ETL for PSCs on aluminum doped zinc oxide (AZO) substrate. AZO is abundant, environment friendly and low cost transparent conducting electrodes for optoelectronic devices. Nonetheless, PSCs based on AZO substrate is reported with relative low PCE of ~13% so far [20, 21], much lower than its ITO and FTO counterparts. The SnO_2-rGO were prepared through spin-coating SnO_2 and rGO mixed solution on the AZO substrate and annealing at 180 °C in air. The rGO possesses excellent charge transport properties, and rGO has proven compatibility with metal oxides [22–24]. However, it has been reported previously that the amount of rGO would affect the photocatalytic properties of the SnO_2-rGO suspension solution [25]. It is suspected that with the right amount of rGO in the composite layer, the rGO would enhance the electron transport behavior while constrain its photodegradation effect on the perovskite thin film.In this study, it is found that the addition of the right amount rGO in the SnO_2 layer effectively reduce electron trap states and passivate the AZO substrate, making the device more stable under the continuous solar illumination compared to pristine SnO_2. The device based on the 3 wt% rGO mass loading in SnO_2 ETL can reach a PCE of 16.87% with reduced hysteresis.

2. Experiment

The AZO glass ($R \approx 10\ \Omega\ \mathrm{sq}^{-1}$, $T \approx 85\%$) was cleaned by deionized water, acetone, ethanol sequentially, and dried by nitrogen purging. Before depositing the SnO_2 layer, the AZO glass was treated by UV-Ozone for 10 min The SnO_2 precursor was purchased from Alfa Aesar (tin oxide, 15% in H_2O)). The SnO_2 precursor was diluted by H_2O to 3%. The rGO nanosheet (diameter ≈0.5–5 *u*m, thickness ≈0.8–1.2 nm) was dissolved in GBL with 1 mg ml^{-1}, and then mixed with SnO_2 solution. The prepared suspension solution with different rGO mass percentage (1 wt%, 3 wt%, 5 wt%) were added to the SnO_2 solution to form our final precursor. The mixed precursor is stable over weeks without any precipitation. The ETL precursor were spin-coated at 3000 rpm for 30 s, followed by annealing at 180 °C for 30 min. The thickness of films were evaluated by using an alpha-step profiler, as shown in figure S1 (available online at stacks.iop.org/NANO/30/075202/mmedia), the average thickness of the resulted ETLs were ~37 nm. The results show that the introduction of a small amount of rGO has insignificant influence on the thickness of perovskite films. For the perovskite layer, 159 mg CH_3NH_3I and 461 mg of PbI_2 were dissolved in 72 ml of DMSO and 640 ml of DMF solution. The perovskite solution was spin-coated on the SnO_2 transfer layer at 4000 rmp for 10 s, and then annealed at 70 °C for 10 min and at 100 °C for another 10 min. The HTM solution was preparation by dissolving 72.3 mg Sprio-OMeTAD in 1 ml chlorobenzene, 18 *u*l Lithium salt solution (520 mg ml^{-1} dissolved in acetonitrile) and 28 *u*l 4-tert-Butylpyridine were added to Sprio-OMeTAD solution. Finally, 80 nm of gold was deposited through a shadow mask with 0.1 cm^2 by thermal evaporation. In addition, the PL spectrum were recorded under excitation at 480 nm, and time-resolved photoluminescence (TPRL) collected excitation at 532 nm, measurements were made by using perovskite film deposited on glass/ETLs substrate with room temperature.

3. Results and discussion

Figure 1(a) shows the device structure of AZO/SnO_2-rGO/$CH_3NH_3PbI_3$/Sprio-OMeTAD/Au, and schematic view of SnO_2-rGO mixture. Figure 1(b) is a cross-sectional SEM image illustrates the fabricated device. The perovskite layer consists of the compact microcrystals with the grain size of several hundred nanometers. A uniform SnO_2-rGO film of ~30 nm forms at the bottom of the AZO substrate. In order to identify the impact of the rGO content on harvesting of the perovskite layer, the optical transmittance of SnO_2 and SnO_2-rGO were measured as a function of rGO content as shown in figure S2. The transmittance decreased with increasing rGO content. It is concluded that excess rGO content would block the light absorption of $SnO_{2,}$ and encourage electron–hole recombination [26]. Furthermore, we monitored the degradation of perovskite layers deposited on SnO_2-rGO. Specifically, optical transmittance spectra of perovskite thin films on SnO_2-rGO coated substrate were monitored against time in ambient environment with temperature of 25 °C and relative humidity of 50%. The results were presented in the figure S3. Initially, the as deposited perovskite films exhibited black color (figure S3e) and a significant light absorption edge at about 780 nm. It is apparent that the color of the perovskite film on SnO_2 layer become yellowish after 120 h, revealing very poor stability of the perovskite on SnO_2 substrate. In contrast, perovskite films with SnO_2-rGO (1 wt%) and SnO_2-rGO (5 wt%) shows a slower color changing rate. It is worth to note that only slight degradation can be observed for perovskite films deposited on SnO_2-rGO (3 wt%) after 120 h (figure S3e). To quantitative the degradation rate, we compared the light transmittance value at the 800 nm ($T_{800\ \mathrm{nm}}$) and the 750 nm ($T_{750\ \mathrm{nm}}$) near the perovskite bandgap absorption edge. The sample with SnO_2-rGO (3 wt%) shows the highest $T_{800\ \mathrm{nm}}/T_{750\ \mathrm{nm}}$ value against time, indicating perovskite thin film on SnO_2-rGO (3 wt%) has the best stability under testing condition among these samples (figure S3f). In addition, the average surface roughness of these SnO_2 films on the AZO substrates were also characterized by atomic force microscope, which is shown in figure S4. The AZO/SnO_2-rGO (3 wt%) surface shows the lowest rms roughness (~58.1 nm), which is lower than the AZO/SnO_2 substrate surface. To obtain optimal doping concentration, different amount of rGO suspension solution, with different mass percent (0, 1, 3, 5 wt%), were added into SnO_2 solution (figure 1(c)).

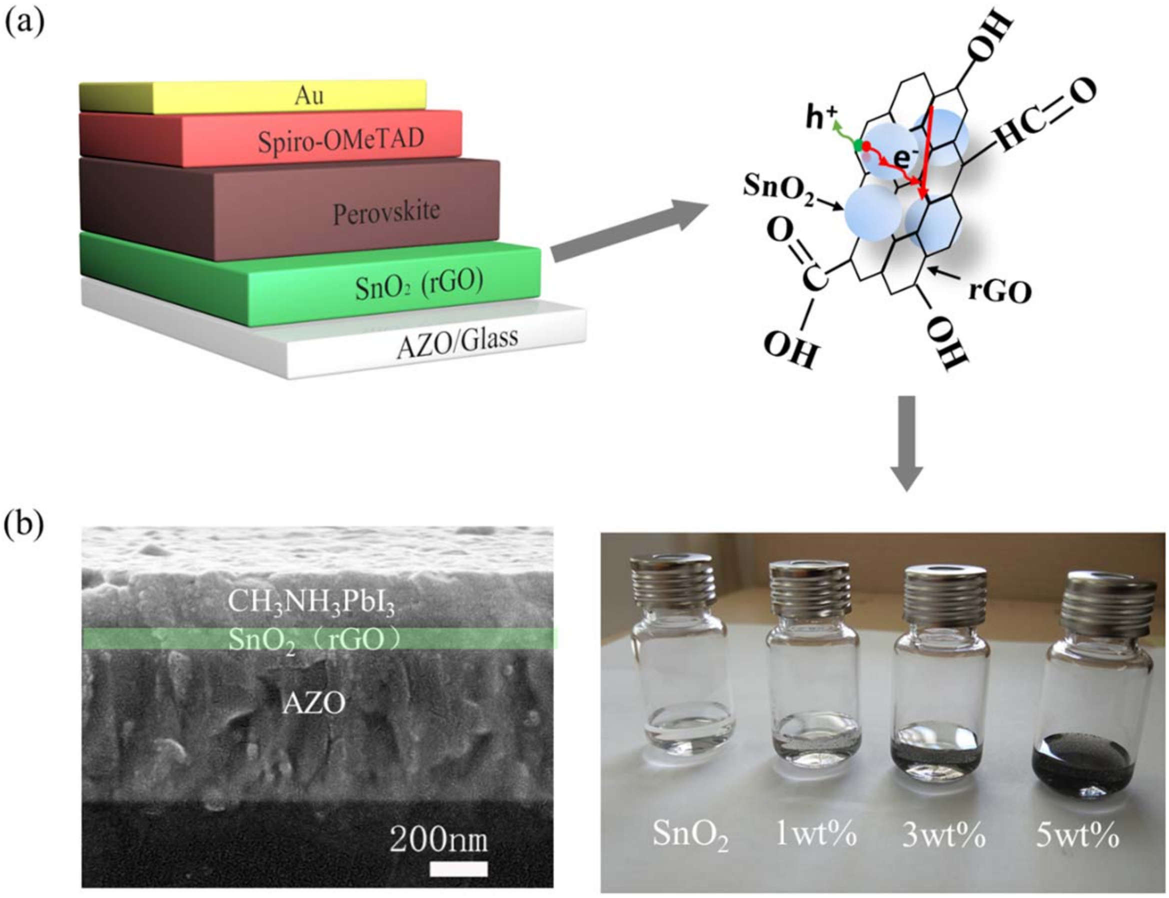

Figure 1. (a) Schematic representation of the typical full device structure; (b) cross-sectional SEM image of a complete photovoltaic device based on the AZO/SnO_2-rGO/$CH_3NH_3PbI_3$ structure (scale bar: 200 nm); (c) the prepared SnO_2-rGO precursor with rGO mass loading of 0, 1, 3 and 5 wt%.

Figures 2(a) and (b) compares the photocurrent density–voltage (*J*–*V*) characteristics under AM1.5G illumination and the external quantum efficiencies of the champion PSCs with SnO_2-rGO (3 wt%) and with pristine SnO_2, respectively. For the champion cells, the J_{sc} increases from 21.45 to 22.57 mA cm^{-2}, and the fill factor increase from 57% to 73%, due to the incorporation of rGO. As a result, the overall PCE is enhanced from 13.9% to 16.87% (table S1). Additionally, in the *J*–*V* characteristic (figure S5), the extracted series resistance (R_s) of the SnO_2-rGO based device is ~3.78 Ω cm^2, which is smaller than that of the SnO_2 based device (7.5 Ω cm^2). The lower R_s of the SnO_2-rGO ETL can be ascribed to the higher electron mobility than that of the pure SnO_2 ETL. Meanwhile, the shunt resistance (R_{sh}) for the SnO_2-rGO device is 2.69 kΩ cm^2, much larger than that of the SnO_2 device (204 Ω cm^2), indicating a suppression of the leakage current and reduction of recombination losses in the SnO_2-rGO device under illumination.

The external quantum efficiency (EQE) spectra of the SnO_2-rGO and SnO_2 devices are shown in the figure 2(b), presenting EQE values higher than 70% for wavelength between 450 and 750 nm in both cells. Although the integrated J_{SC} is a bit lower than the results obtain from the *J*–*V* characteristics due to the spectrum mismatch between equipment and theoretical spectra data, the overall J_{SC} variation trend of the two devices match well with the *J*–*V* measurement results [27]. The device with SnO_2-rGO film exhibits higher EQE, compared to the SnO_2 based PSC, leading to a higher integrated J_{SC}. Since the perovskite films grown on SnO_2-rGO film and SnO_2 film exhibits UV–vis absorbance (figure S6), it can be inferred that the J_{sc} enhancement mainly derives from the improved electron transfer efficiency via rGO at the perovskite and ETL interface. It is found that the additive of 3 wt% rGO loading into SnO_2 precursor can significantly improve the performances of the devices. In fact, the device doped with 3 wt% rGO in SnO_2 presents the best results, with an averaged PCE of ~16.7% as shown in the statistic results in figure 2(c). Figure 2(d) is a histogram of PCE over 20 devices fabricated on the SnO_2 and SnO_2-rGO, obtaining that the devices based on the SnO_2-rGO an average PCE of 16.4 ± 0.4%. Hence, it is deduced that the incorporation of rGO bring a more efficiency and stable PSCs.

To further investigate the charge-transport kinetics at the SnO_2-rGO/$MAPbI_3$ interface, the steady-state PL spectra and TRPL measurement are employed. The PL spectra is collected from perovskite films fabricated on glass/ETLs in the figure 3(a), PL peak are observed about 780 nm for both perovskite films with or without rGO. The SnO_2-rGO/$MAPbI_3$ film has a much lower PL quantum yield than the SnO_2/$MAPbI_3$ film, indicating a higher charge extraction rate across the

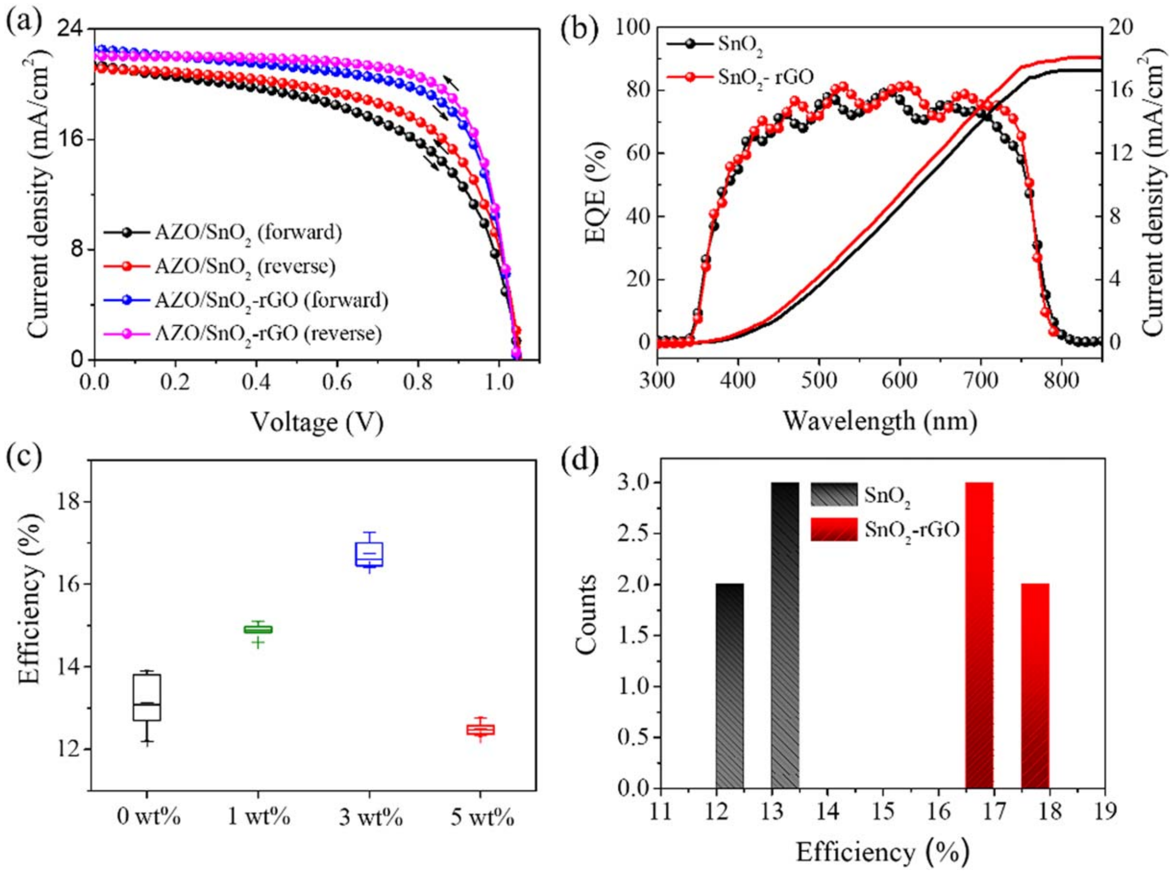

Figure 2. (a) *J–V* curves in forward bias and reverse bias for the best-performing PSC solar cell with the doping concentration of 3 wt% (SnO_2-rGO) and the reference one (SnO_2); (b) EQE spectra of the optimal SnO_2 and SnO_2-rGO based devices; (c) PCE distribution of the devices with and without rGO in the SnO_2 ETL; (d) histograms of PCE with the doping concentration of 3 wt% (SnO_2-rGO) and the reference SnO_2 ETL.

interface between the SnO_2-rGO and $MAPbI_3$. The TRPL was measured, adopting the same structures as used for the PL measurements. The TRPL results of devices based on SnO_2 and SnO_2-rGO ETL are presented in figure 3(b). The two TRPL curves can be fitted by a bi-exponential equation [27, 28]:

$$f(t) = A_1 e^{-t/\tau_1} + A_2 e^{-t/\tau_2} + B, \quad (1)$$

where the terms A_1, A_2 are the decay amplitude, B is the constant for the base-line offset, τ is the decay time. The decay portion including a fast decay (τ_1) component reflects the quenching of free carriers in the interface between the perovskite and ETL, and a slow decay (τ_2) component represents the recombination of free carriers in radiative channels [28]. The PL decay of the perovskite deposited on the SnO_2 film presents a fast decay lifetime (τ_1) of 31 ns and a slow decay lifetime (τ_2) of 6.4 ns. In contrast, for the SnO_2-rGO/$MAPbI_3$ film, the fast decay lifetime and the slow decay lifetime are both shortened, with extracted values of 23 ns and 5.2 ns respectively. The faster PL quenching rate indicates a faster charge transfer rate at the SnO_2-rGO/$MAPbI_3$ junction interface. The PL spectra and the TPRL results are consistent with our finding from *I–V* and EQE measurements, suggesting that the addition of the rGO in the SnO_2 ETL, the J_{sc} is improved.

A space-charge limited current (SCLC) measurements were also carried out to evaluate the electron mobility of SnO_2-rGO ETL, the results of which are shown in figure 3(c). We have fabricated device with AZO/SnO_2-rGO/$MAPbI_3$/PCBM/BCP/Au configuration for electron transport investigation. The *I–V* curves from electron-transport-only measurements can be cataloged into three regions according to the value of the exponent n [29], i.e. $n = 1$ is the ohmic region, $n = 2$ is the SCLC region, and the intermediate region between 1 and 2 is the trap-filled limited region. In the SCLC region, the electron mobility of the PSCs with SnO_2-rGO film can be evaluated on the basis of the Mott–Gurney law [29]

$$J = \frac{9}{8}\varepsilon_0 \varepsilon \mu \frac{V^2}{d^3}, \quad (2)$$

where V is the applied voltage, d is the thickness of the ETLs, ε is the dielectric constant of the SnO_2 (12.5) film and μ is the electron mobility. The estimated electron mobility of 3.3×10^{-3} cm^2 V^{-1} s^{-1} can be obtained from the equation (2) from the device based SnO_2-rGO film, which is about 5 times higher than that of the SnO_2 based device (7×10^{-4} cm^2 V^{-1} s^{-1}). The magnitudes of our mobility values are in the same order to those reported in reference [30]. The SCLC results further confirms that the photogenerated charge carriers are more efficiently transferred via the SnO_2-rGO ETL than the pristine SnO_2 ETL.

Dark current measure is a method to evaluate charge carrier loss through leakage pathways and the recombination of free

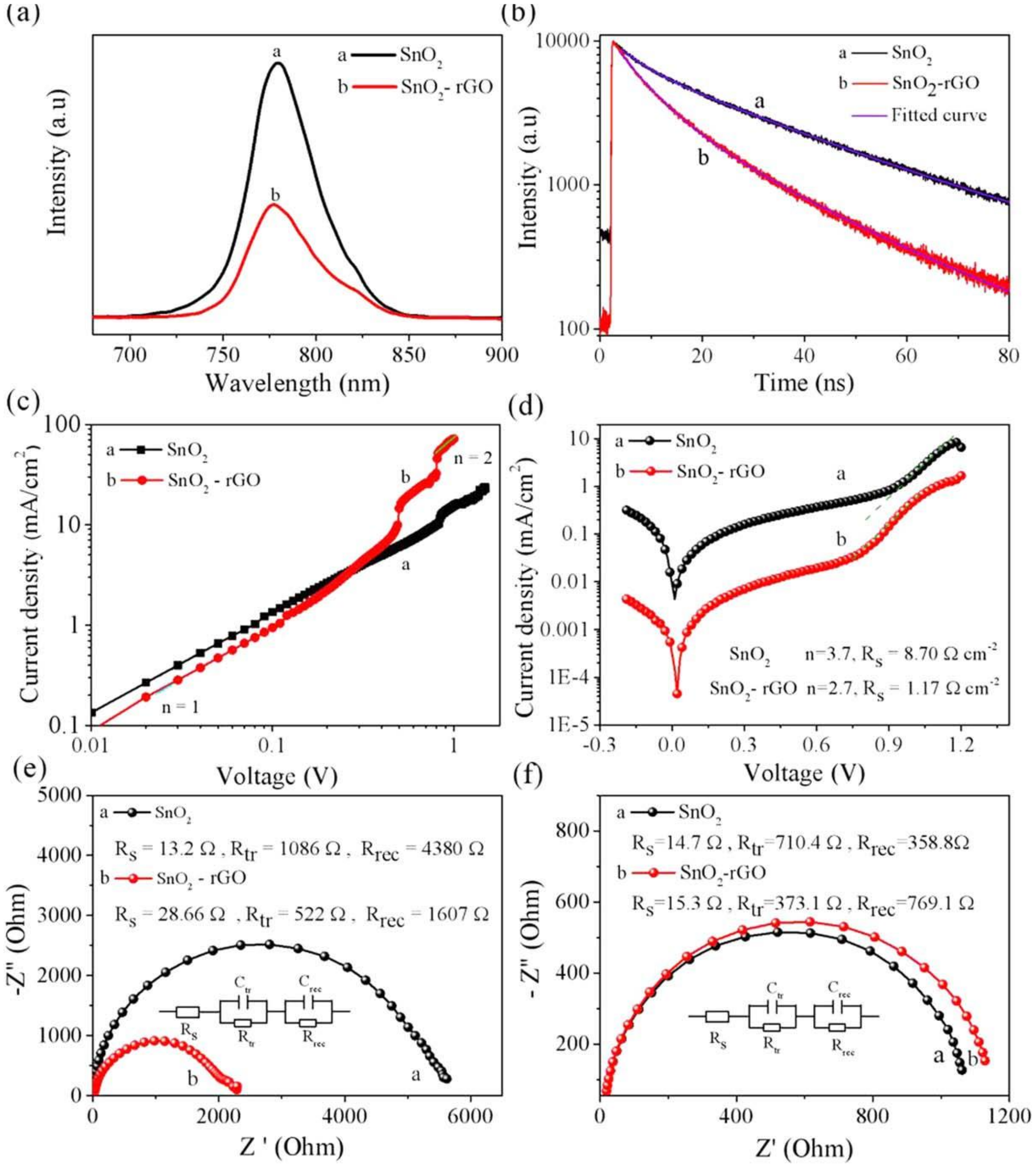

Figure 3. (a) Photoluminescence emission spectra of AZO/SnO_2/perovskite and AZO/SnO_2-rGO/perovskite; (b) TRPL of $CH_3NH_3PbI_3$ contacted with different interfaces: SnO_2, SnO_2-rGO; (c) *I–V* characteristics of the AZO/SnO_2/$CH_3NH_3PbI_3$/PCBM/BCP/Au and AZO/SnO_2-rGO/CH_3NH_3 PbI_3/PCBM/BCP/Au; (d) *J–V* curves for the best-performing PSC solar cell with the doping concentration of 3 wt% (SnO_2-rGO) and the reference one (SnO_2) in the dark. Electrochemical impedance spectroscopy of PSC based on SnO_2 and SnO_2-rGO films under the dark (e) and illumination condition(f).

carriers in devices. Figure 3(d) shows the dark *I–V* curves for the best PSCs with SnO_2 and with SnO_2-rGO, the *J–V* characteristics in dark can be described by the Shockley diode equation [31]:

$$J = J_0\left[\exp\left(\frac{qV}{nKT}\right) - 1\right] \tag{3}$$

where J_0 is the saturation current density, V is the applied voltage, n is the ideality factor, T is the temperature and K is the Boltzaman constant. The dark curves show typical diode properties, with a transition to the SCLR at the build in voltage (V_{bi}). The ideality factor can be determined from the slope of the exponential regime on the semi-logarithmic plot and can be denoted as:

$$n = \left(\frac{kT}{q}\frac{\partial \ln J}{\partial V}\right)^{-1}. \tag{4}$$

In the equation (4), n of the device with SnO_2 has a value of 3.7, which is higher than that of the device with SnO_2-rGO

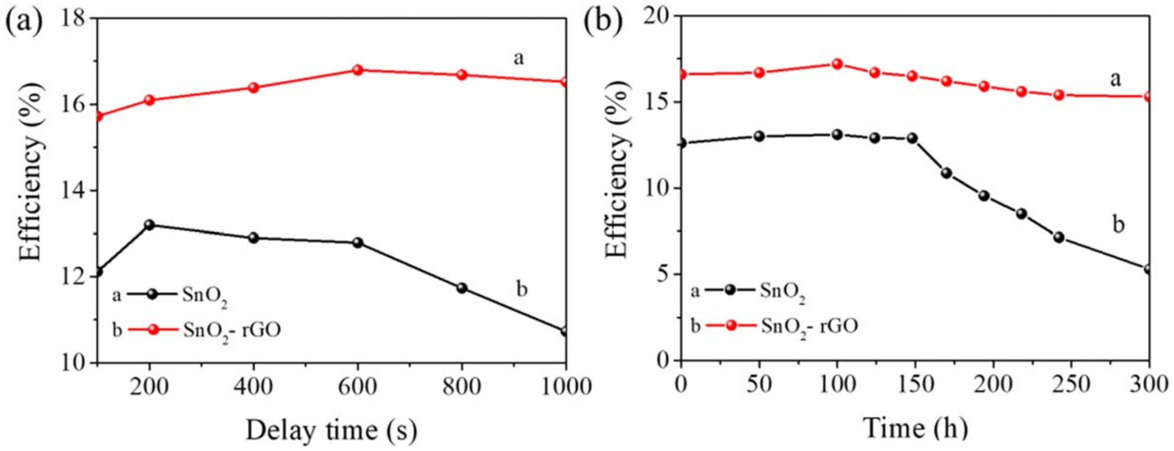

Figure 4. (a) SnO_2 (curve a) and SnO_2-rGO (curve b) ETLs based PSCs under continuous solar illumination; (b) devices stability with SnO_2 and SnO_2-rGO ETL in the glove box without capsulation.

of 2.7. n extracted value are significantly large than 1 for both devices, demonstrating that trap assisted recombination plays a mass of role in the recombination process [30]. However, PSC based SnO_2-rGO ETL showed an n value and a R_s (1.17 $\Omega\,cm^2$) smaller with regard to the SnO_2 ETL (8.7 $\Omega\,cm^2$). Suggesting a decreased trap state density at AZO/SnO_2 interface when rGO is added to SnO_2. According to equation (3), it can be obtained that the J_0 of the device without rGO is 6.32×10^{-5} mA cm^{-2}, which is one order of magnitude large than that of the device with SnO_2-rGO is 1.3 $\times 10^{-5}$ mA cm^{-2}. This decrease in J_0 indicates that carrier recombination is suppressed by the use of rGO. It is suspected that the rGO helps in forming a more compact ETL by filling the voids that originated from SnO_2 nanoparticle aggregations, thus reducing the leakage paths by preventing the perovskite layer from direct contacting the AZO surfaces.

To further reveal the role of the rGO in SnO_2 film, electrochemical impedance spectroscopy analysis was applied to the devices with SnO_2 and SnO_2-rGO ETL under dark and illumination conditions with a bias voltage of 0.1 V. The Nyquist curves of both devices under dark condition have been plotted in figure 3(e), with an equivalent circuit shown as inset diagram. The resistance R_s can be extracted from the intersections of these arcs, corresponding to the resistance of AZO/ETLs and HTLs/Au. The resistance R_{tr} from the high frequency arc regime mostly attributed to the transport resistance of ETLs/Perovskite/Spiro-OMeTAD layers [32, 33]. The fitted value of the ohmic resistance (R_s) and charge transfer resistance (R_{tr}) in the figure 3(e). The R_{tr} of the device based on SnO_2 PSCs is 1086 Ω, and the R_{tr} of the device based on SnO_2-rGO is 522 Ω. The device based SnO_2-rGO exhibits the smaller charge transfer resistance suggests that electron transport faster at the SnO_2-rGO/Perovskite interface. Figure 3(f) shows the Nyquist plots of both SnO_2 and SnO_2-rGO based device under illumination condition. The resistance from lower frequency arc is related to the recombination resistance (R_{rec}). The R_{rec} of the SnO_2-rGO device is 769.1 Ω, and the R_{rec} of the SnO_2 device is 358.8 Ω. The calculated values of the charge transfer resistance (R_{tr}) using the inset equivalent circuit is 373.1 Ω for the device based on SnO_2-rGO, which is much lower than the device based on SnO_2 with 710.4 Ω. The carrier diffusion length L_d can be estimated by [34]

$$L_d = \left(\frac{R_{rec}}{R_{tr}}\right)^{\frac{1}{2}} L, \qquad (5)$$

where R_{rec} is the recombination resistance, R_{tr} is the charge transfer resistance, L is the layer thickness. According to the equation (5), with similar L in the devices, the large R_{rec} and small R_{tr} in solar cell decrease the possibility for electron–hole recombination.

In order to confirm light stability, the light stability measurements on the PSC were investigated. The J–V measure of PSC with SnO_2-rGO electron transfer layer under different continuous illumination time from 100 to 1000 s were measured and presented in the figure 4(a). The SnO_2 based PSC degrades with time rapidly, with PCE decreasing from ~12% to 11% within 1000 s. The most prominent decay is obtained in the plot of V_{oc} (in the figure S7). In contrast, upon light exposure, the SnO_2-rGO device remains more stable with PCE above 16% for more than 1000 s. The stability of devices was also tested as a function of storage time in the glove box without capsulation. The PCE is plotted independently in the figure 4(b) to reveal the stability of the devices clearly. The SnO_2-rGO device, the PCE keep 80% after 300 h while PCE of the SnO_2 device drops down to <50%. It is worth noting that the stability of PSCs was tested under AM. 1.5G as light source. The results confirm that the SnO_2-rGO based PSCs is more stable than the SnO_2 device.

The enhanced stability of PSC may be ascribed to the passivation effect of rGO at the interface. For example, the surface of the AZO and low temperature solution processed SnO_2 contain many trap states originated from oxygen vacancies [35], which leads to decomposed of perovskite at the interface and increase carrier recombination. The rGO is suspected to distribute at the boundary of SnO_2 nanocrystals and passivate the electron traps of the SnO_2 and the AZO surface.

4. Conclusion

In this study, we have synthesized a new way to improve the performance of planar n-i-p PSCs by adding rGO of 3 wt% into SnO_2. The addition of rGO resulted in a high efficiency of 16.87% with a very reduced hysteresis, and the devices deposited on the AZO substrate and treated below 180 °C. In addition, the increased J_{sc} of the device based on SnO_2-rGO, which attributes to effective electron extraction from perovskite to AZO. On the other hand, the rGO doped SnO_2 can effectively improve the device stability is due to the stabilization of AZO/SnO_2 interface. The introduction of rGO in SnO_2 is a simple and effective way to improve device performances.

Acknowledgments

This work is financially supported by the National Key Research and Development Program of China (2016YFA0202002), and the Shenzhen Science and Technology Innovation Foundation (JCYJ20160229122349365). Chuan Liu would like to acknowledge Science and Technology Program of Guangdong Province (Grant No. 2015B090924001), Guangdong Natural Science Funds for Distinguished Young Scholars (Grant No. 2016A030306046).

ORCID iDs

Jun Chen https://orcid.org/0000-0001-7397-2714
Qing Dai https://orcid.org/0000-0002-1750-0867
Hang Zhou https://orcid.org/0000-0002-0472-9515

References

[1] NREL B R-cell E. (nrel.gov/ncpv/images/efficiencychart.jpg)

[2] Xing G, Mathews N, Sun S, Lim S S, Lam Y M, Grätzel M, Mhaisalkar S and Sum T C 2013 Long-range balanced electron- and hole-transport lengths in organic-inorganic $CH_3NH_3PbI_3$ *Science* **342** 344–7

[3] Yettapu G R, Talukdar D, Sarkar S, Swarnkar A, Nag A, Ghosh P and Mandal P 2016 THz conductivity within colloidal $CsPbBr_3$ perovskite nanocrystals: remarkably high carrier mobilities and large diffusion lengths *Nano Lett.* **16** 4838–48

[4] Kojima A, Teshima K, Shirai Y and Miyasaka T 2009 Organometal halide perovskites as visible-light sensitizers for photovoltaic cells *J. Am. Chem. Soc.* **131** 6050–1

[5] Ito S, Tanaka S, Manabe K and Nishino H 2014 Effects of surface blocking layer of Sb_2S_3 on nanocrystalline TiO_2 for $CH_3NH_3PbI_3$ perovskite solar cells *J. Phys. Chem.* C **118** 16995–7000

[6] Xu Y, Liu T, Li Z S, Feng B J, Li S, Duan J X, Ye C, Zhang J and Wang H 2016 Preparation and photovoltaic properties of perovskite solar cell based on ZnO nanorod arrays *Appl. Surf. Sci.* **388** 89–96

[7] Mahmood K, Swain B S and Amassian A 2015 16.1% efficient hysteresis-free mesostructured perovskite solar cells based on synergistically improved ZnO nanorod arrays *Adv. Energy Mater.* **5** 150056

[8] Cheng Y, Yang D, Xiao J, Xue Q, Li H W, Guan Z, Yip H L and Tsang S W 2015 Decomposition of organometal halide perovskite films on zinc oxide nanoparticles *ACS Appl. Mater. Interfaces* **7** 19986–93

[9] Dong J *et al* 2014 Impressive enhancement in the cell performance of ZnO nanorod-based perovskite solar cells with Al-doped ZnO interfacial modification *Chem. Commun.* **50** 13381–4

[10] Ko Y, Kim Y R, Jang H, Chanyong L, Man G and Yongseok J K 2017 Electrodeposition of SnO_2 on FTO and its application in planar heterojunction perovskite solar cells as an electron transport layer *Nanoscale Res. Lett.* **12** 498

[11] Murugadoss G, Kanda H, Tanaka S, Hitoshi N, SeigoIto H and Tomokazu U 2016 An efficient electron transport material of tin oxide for planar structure perovskite solar cells *J. Power Sources* **307** 891–7

[12] Barbé J *et al* 2017 Amorphous tin oxide as a low-temperature-processed electron-transport layer for organic and hybrid perovskite solar cells *ACS Appl. Mater. Interfaces* **9** 11828–36

[13] Song J, Zheng E, Bian J, Wang X, Tian W, Sanehira Y and Miyasaka T 2015 Low temperature SnO_2-based electron selective contact for efficient and stable perovskite solar cells *J. Mater. Chem.* A **3** 10837–44

[14] Yang J, Siempelkamp B D, Mosconi E, Angelis F D and Kelly T L 2015 Origin of the thermal instability in $CH_3NH_3PbI_3$ thin films deposited on ZnO *Chem. Mater.* **27** 4229–36

[15] Jiang Q, Zhang L, Wang H, Yang X, Meng J, Liu H, Yin Z, Wu J, Zhang X and You J 2016 Enhanced electron extraction using SnO_2 for high-efficiency planar-structure $HC(NH_2)_2PbI_3$-based perovskite solar cells *Nat. Energy* **2** 16177

[16] Tan H *et al* 2017 Efficient and stable solution-processed planar perovskite solar cells via contact passivation *Science* **355** 722–6

[17] Yang G *et al* 2017 Reducing hysteresis and enhancing performance of perovskite solar cells using low-temperature processed Y-doped SnO_2 nanosheets as electron selective layers *Small* **13** 1601769

[18] Bai Y, Fang Y, Deng Y, Wang Q, Zhao J, Zheng X, Zhang Y and Huang J 2016 Low temperature solution-processed Sb: SnO_2 nanocrystals for efficient planar perovskite solar cells *ChemSusChem.* **9** 2686–91

[19] Nouri E, Mohammadi M R and Lianos P 2016 Impact of preparation method of TiO_2-RGO nanocomposite photoanodes on the performance of dye-sensitized solar cells *Electrochim. Acta* **219** 38–48

[20] Zhao X, Shen H, Zhang Y, Li X, Zhao X, Tai M, Li J and Lin H 2016 Aluminum-doped zinc oxide as highly stable electron collection layer for perovskite solar cells *ACS Appl. Mater. Interfaces* **8** 7826–33

[21] Li X, Ye W, Zhou X, Huang F and Zhong D 2017 Increased efficiency for perovskite photovoltaics based on aluminum-doped zinc oxide transparent electrodes via surface modification *J. Phys. Chem.* C **121** 10282–8

[22] Kumar P V, Bernardi M and Grossman J C 2013 The impact of functionalization on the stability, work function, and photoluminescence of reduced graphene oxide *ACS Nano.* **7** 1638–45

[23] Huang X, Qi X, Boey F and Zhang H 2012 Graphene-based composites *Chem. Soc. Rev.* **41** 666–86

[24] Byranvand M M, Kim T, Song S, Kang G, Ryu S U and Park T 2017 p-type CuI islands on TiO_2 electron transport layer for a highly efficient planar-perovskite solar cell with negligible hysteresis *Adv. Energy Mater.* **8** 1702235

[25] Seema H, Christian K K, Chandra V and Kim K S 2012 Graphene-SnO_2 composites for highly efficient photocatalytic degradation of methylene blue under sunlight *Nanotechnology* **23** 355705

[26] Chen Y C, Katsumata K I, Chiu Y H, Okada K, Matsushita N and Hsu Y J 2015 ZnO–graphene composites as practical photocatalysts for gaseous acetaldehyde degradation and electrolytic water oxidation *Appl. Catal.* A **490** 1–9

[27] Ponseca J C S *et al* 2014 Organometal halide perovskite solar cell materials rationalized: ultrafast charge generation, high and microsecond-long balanced mobilities, and slow recombination *J. Am. Chem. Soc.* **136** 5189–92

[28] Dong Q, Fang Y, Shao Y, Mulligan P, Qiu J, Cao L and Huang J 2015 Solar cells. Electron–hole diffusion lengths >175 *u*m in solution-grown $CH_3NH_3PbI_3$ single crystal *Science* **347** 967–70

[29] Wetzelaer G J, Scheepers M, Sempere A M, Momblona C, Ávila J and Bolink H J 2015 Trap-assisted non-radiative recombination in organic–inorganic perovskite solar cells *Adv. Mater.* **27** 1837–41

[30] Xie J *et al* 2017 Enhanced electronic properties of SnO_2 via electron transfer from graphene quantum dots for efficient perovskite solar cells *ACS Nano* **11** 9176–82

[31] Agresti A, Pescetelli S, CinàL, Konios D, Kakavelakis G, Kymakis E and Carlo A D 2016 Efficiency and stability enhancement in perovskite solar cells by inserting lithium-neutralized graphene oxide as electron transporting layer *Adv. Funct. Mater.* **26** 2686–94

[32] Nouri E, Mohammadi M R, Xu Z X, Dracopoulos V and Lianos P 2018 Improvement of the photovoltaic parameters of perovskite solar cells using a reduced-graphene oxide-modified titania layer and soluble copper phthalocyanine as a hole transporter *Phys. Chem. Chem. Phys.* **20** 2388–95

[33] Bisquert J, Santiago F F, Sero I M, Belmonte G G and Gimenez S 2009 Electron lifetime in dye-sensitized solar cells: theory and interpretation of measurements *J. Phys. Chem.* C **113** 17278–90

[34] Gonzalez-Pedro V, Juarez-Perez E J, Arsyad W S, Barea E M, Fabregat-Santiago F, Mora-Sero I and Bisquert J 2014 General working principles of $CH_3NH_3PbX_3$ perovskite solar cells *Nano Lett.* **14** 888–93

[35] Park M, Kim J Y, Son H J, Lee C H, Jang S S and Ko M J 2016 Low-temperature solution-processed Li-doped SnO_2 as an effective electron transporting layer for high-performance flexible and wearable perovskite solar cells *Nano Energy* **26** 208–15